Revue des Composites et des Matériaux Avancés-Journal of Composite and Advanced Materials
Vol. 35, No. 4, August, 2025, pp. 643-653
Journal homepage: http://iieta.org/journals/rcma

Development and Characterization of Antibacterial Polymer Blends Composed of PVA, PAAm, and PEG Integrated with Carbon Nanotubes

Khansaa Saleem Sharba[1], Akeel Shakir Alkelaby[1*], Khalid Haneen Abass[2]

[1] The General Directorate of Education in Babil, Ministry of Education, Babylon 51001, Iraq
[2] Physics Department, College of Education for Pure Sciences, University of Babylon, Babylon 51002, Iraq

Corresponding Author Email: akeelshakir@gmail.com

https://doi.org/10.18280/rcma.350406

Received: 27 June 2025
Revised: 28 July 2025
Accepted: 20 August 2025
Available online: 31 August 2025

Keywords:
PVA-PEG:CNT, electrical properties, structural properties, E. coli Bacteria

ABSTRACT

The PVA-PAAm-PEG polymer blends and their corresponding nanocomposite films were synthesized using the solution casting method, with carbon nanotubes (CNTs) added in varying concentrations of 0.005 g, 0.010 g, 0.015 g, and 0.020 g. Structural characterization was carried out through FTIR spectroscopy, which revealed that the interactions were predominantly physical, indicating the absence of new chemical bonds or interatomic interactions. SEM analysis confirmed this finding by demonstrating a uniform dispersion of CNTs within the polymer matrix. Through the evaluation of their absorption spectra over the 200–800 nm wavelength range, the optical properties were investigated. The results indicated a progressive increase in optical absorption with higher CNT concentrations. Concurrently, the optical band gap was observed to decrease from 4.8 eV to 3.6 eV. The refractive index similarly exhibited increasing levels of CNT incorporation. Both the dielectric constant and dielectric loss were found to increase with higher CNT concentrations, while they showed a decrease with higher applied electric field frequencies. On the contrary, AC conductivity demonstrated enhancement with increasing frequency, particularly at 102 Hz. Additionally, the antibacterial properties of the nanocomposites were tested against *Escherichia coli* (*E. coli*), revealing augmented antibacterial activity as the CNT concentration increased. This highlights the potential application of these nanocomposites in antimicrobial technologies.

1. INTRODUCTION

Nanocomposites hold significant relevance within the realm of polymer nanomaterials due to their unique and highly adaptable physicochemical properties [1]. Advances in this field primarily concentrate on optimizing interfacial interactions and achieving a uniform dispersion of nanofillers throughout the polymer, matrix—crucial factors for enhancing the overall functionality and performance of these materials [2]. The augmentation of polymer characteristics is closely tied to the inclusion of nanomaterials, which markedly boost the functional capabilities of nanocomposites [3].

Polymeric nanocomposites have garnered substantial attention from researchers because of their remarkable properties, including a high strength-to-weight ratio, superior corrosion resistance, cost-effectiveness, and adaptability for forming intricate shapes [4]. To enhance fundamental attributes, including mechanical robustness, electrical conductivity and thermal conductivity, various nanoscale fillers are incorporated into these materials. The success of these enhancements relies on the careful selection of fillers—ranging from fibers to different particulate types—based on the specific requirements and desired application improvements [5]. Polymers themselves are broadly divided into natural and synthetic categories. Natural polymers include substances such as proteins, cellulose, starch, and rubber. Conversely, synthetic polymers encompass a wide range of materials like polyvinyl chloride (PVC), nylon, polyethylene, polypropylene, polyester, polycarbonate, among others. Each polymer type offers distinct advantages, making them well-suited for diverse industrial and technological applications [6].

Polyvinyl alcohol (PVA), a water-soluble and biodegradable polymer, is derived from the hydrolysis of polyvinyl acetate and is readily degradable by organic organisms [7]. Its biocompatibility and non-toxic attributes have established PVA as a material of significant interest within the biomedical field, particularly in the development of drug delivery systems, highlighting its relevance across various biological applications [8]. This lightweight, highly crystalline polymer exhibits an abundance of hydroxyl (-OH) groups, which confer distinctive physical and chemical properties, notably its capacity for film formation [9]. The molecular architecture of PVA comprises a carbon backbone with hydroxyl groups bonded via methylene carbon atoms. These hydroxyl groups serve as both hydrogen bond donors and acceptors, enhancing PVA's suitability for synthesizing polymer blends and composites [10]. Owing to its adaptability and broad scope of utility, PVA has been rigorously studied

for a diverse range of applications, encompassing electrochemical devices, sensors, medical apparatuses, and fuel cells [11]. Its exceptional properties encompassing high mechanical strength, outstanding resistance to corrosion, and superior thermal stability—distinguish it from conventional polymers [12].

Polyacrylamide (PAAm) is a highly adaptable hydrophilic polymer recognized for its broad utility across numerous industrial sectors. Over recent years, PAAm and its derivatives have garnered considerable research interest due to their exceptional durability under significant molecular stress, water solubility without the generation of harmful byproducts, and inherently non-toxic nature. PAAm copolymers, synthesized with various hydrophilic monomers and metal salts, are extensively utilized in industries such as mining, water treatment, and other process-driven operations [13]. One of PAAm's key roles is its capacity to enhance the viscosity of aqueous solutions, polyamide-based systems, and fixed acrylic materials. Structurally, the polymer is defined by amine and carboxyl functional groups along its dry chains, which facilitate extensive hydrogen bonding between polymer strands. This bonding contributes to the development of robust polyamide networks, thereby boosting material stability, mechanical strength, and overall performance. While PAAm-based products offer numerous advantageous properties, they are often hindered by relatively low tensile strength, insufficient compressive resistance, and limited elongation [14].

Polyethylene glycols (PEG) constitute a class of highly versatile polymers obtainable in both liquid and solid states, characterized by the chemical formula $H(OCH_2CH_2)_nOH$ [15]. To enhance their elasticity, additional polymers are frequently integrated into their composition. The inclusion of a plasticizer plays a key role in further improving flexibility by reducing intermolecular forces within the polymer chains, thereby decreasing molecular rigidity. Without the presence of plasticizers or complementary polymers, PEG alone lacks the necessary properties for film production [16]. As a water-soluble thermoplastic, PEG possesses a uniquely flexible structure based on C–O–C bonds. It is notable for its excellent the compound exhibits notable solubility in both aqueous and organic media, demonstrating pronounced hydrophilic properties nature, crystallinity, and self-lubricating features. These attributes make PEG a highly preferred polymer with broad applications, particularly in essential fields such as solid polymer electrolytes used for sensors and batteries [17].

Carbon nanotubes (CNTs), a distinct carbon allotrope, are defined by their tubular structures formed from sheets of graphite. Celebrated for their extraordinary properties, CNTs have become highly significant in both nanotechnology and pharmaceutical sciences. Their diameters range within the nanometer scale, while their lengths can stretch to several millimeters, offering a wide variety of electronic, thermal, and mechanical attributes. These specific properties are shaped by parameters such as diameter, length, chirality, twisting configuration, and wall morphology. With an impressive surface area, as well as notable stiffness, strength, and durability, CNTs have garnered considerable interest in pharmaceutical research and applications [18].

Carbon-based nanofillers, known for their ability to optimize material performance even at very low concentrations, stand out in the field of polymer enhancement. Among these, polymer composites infused with CNTs and graphene have achieved widespread application across various scientific and technological disciplines. These fillers significantly elevate the functional properties of polymer matrices, tailoring them to meet specialized requirements [19]. Graphene, in particular, has captured significant attention due to its extraordinary qualities [20]. Sourced from natural graphite, it also offers a more economical option compared to CNTs [21]. Lakouraj et al. [22] developed conductive and corrosion-resistant films using multicomponent aniline-carbazole polymers with the addition of carbon nanotubes. The developed films exhibited improved mechanical properties, corrosion resistance, and good thermal properties. The electrochemical properties of the films were studied using various techniques, and the results demonstrated corrosion resistance and low wear rate. Mi et al. [23] reported that polypropylene (PP) composites with carbon nanotubes (CNTs) were prepared using different methods to provide varying shear strengths. The effects of CNT doping and distribution on the mechanical and electrical properties of these composites were studied. The results showed an increase and improvement in the mechanical and electrical properties. Nassar et al. [24] prepared polyvinyl alcohol (PVA) nanocomposites with carbon nanotubes (CNTs) at different concentrations. The thermal, electrical, and morphological properties of the various composites were studied using various techniques. The nanocomposites were found to exhibit diverse distributions and enhanced thermal and electrical properties. In this research, we will create advanced PVA-PAAm-PEG: CNT nanocomposites, comprehensively analyze their structural, optical and electrical properties, and finally evaluate their antibacterial capabilities.

2. EXPERIMENTAL PART

The polymers used in this study include polyvinyl alcohol (PVA) with molecular wight of 18,000 grams/moles and an purity of 99.0%, derived from Pareek (Barcelona, Spain); Polyacrylamide (PAAm), with the molecular weight of 5×10 g/moles and purity of 99.99%, was supplied by the British Drug House (BDH); And polyethylene glycol (PEG) was obtained from the reagent world, With a molecular weight of 6000 and a purity level of 99.8%, all polymers were utilized in granular form. The nanomaterials used as additives were CNTs (90% purity, 100 nm diameter, and 10 μm length) incorporated in varying percentages.

3. PREPARATION OF PVA-PAAm-PEG: CNT NANOCOMPOSITES

Polymer -nanocomposite films were made dissolving 40% Polyacrylamide (PAAM). In a glass beaker containing 60 ml of distilled water, equipped with a magnetic stirrer for thorough mixing. The solution was stirred vigorously at 90°C for 45 min to ensure the formation of a homogeneous mixture. Then 40% polyvinyl alcohol (PVA) was introduced in the PAAM solution, and continued stirring for one hour at the same temperature to ensure homogenous solution mixture. Next, 20% polyethylene glycol (PEG) was incorporated into a polymer matrix, and the mixture was allowed in front of an hour at 90°C. The temperature of the PVA-PAAm-PEG matrix was adjusted to approximately 25°C as a preparatory step for incorporating various weight ratios of carbon nanotubes (CNTs). Specifically, four formulations with CNT ratios of

0.5, 1.0, 1.5, and 2.0 were sequentially introduced, each undergoing a mixing process of one hour to fabricate the PVA-PAAm-PEG-CNT nanocomposite, as outlined in Table 1. To enhance the dispersion and overall properties of the nanocomposite, ultrasonication was employed—a widely utilized method for ensuring homogeneous distribution of CNTs within solvent systems. This technique generates significant mechanical forces within the solvent, producing cavitation bubbles that effectively facilitate CNT dispersion. The ultrasonication procedure was conducted for a duration of 3 minutes using water as the solvent medium for nanocomposite preparation. They cast each of these ratios within a 5-centimeter diameter Petri dish to create the films and the complete setup is kept in a clean, dust-free environment, allowing the solvent to gradually evaporate at room temperature over a period of seven days. Once this process is complete, the film is gently removed from the petri dish.

Table 1. Summarized the preparation of PVA-PAAm-PEG and PAAm-PVA-PEG:CNT nanocomposites

Smples No.	PVA (g)	PAAm (g)	PEG (g)	CNT (%)
1	0.4	0.4	0.2	0.0
2	0.398	0.398	0.199	0.5
3	0.396	0.396	0.198	1.0
4	0.394	0.394	0.197	1.5
5	0.392	0.392	0.196	2.0

4. DISCUSSION AND RESULTS

The Fourier transform infrared (FTIR) test was used to determine changes in the bonds and the formation of new bonds in the PVA-PAAm-PEG blend. Figure 1 represents the FTIR of PVA-PAAm-PEG:CNT nanocomposites with varying ratios of CNT. Spectra were recorded at room temperature, in a range from 4000-500 cm^{-1}. The observed spectra show the characteristic bands of stretching and bending vibrations of the functional groups present in the composites. In particular, 3290.92 and 3292.57 cm^{-1} around absorption peaks were assigned to the hydroxyl (O-H) stretching vibration in a polymer matrix [25]. The peaks displayed on 2895.29, 2893.09, 2890.43, 2891.25, and 2891.20 cm^{-1} were held responsible for methylene (C-H) stretching mode, while the bands at 1732.71 and 1733.16 cm^{-1} were attributed to carboxylic acid (C=O) stretching [26]. In addition, absorption systems at 1240.67, 1240.68, 1240.61, 1240.40 and 1239.69 cm^{-1} were identified as carbon dioxide (C-O) stretching [27]. The peaks of 1090.50, 1099.82, 1107.07, and 1101.25 cm^{-1} are recognized as carbon-carbon (C-C) stretching vibrations [28]. In particular, FTIR spectra of nano-composites revealed a shift in peak position and variation in shape and intensity compared to pure PVA-PAAm-PEG films. Especially because of interest was the characteristic hydroxyl (O-H) tensile tape close to 3300 cm, usually associated with PVA, absent. Instead, the region performed tops of 3290.92, 3292.57 and 3292.87 cm^{-1}, attributed to (OH) stretching vibrations, are observed. In addition, the peak observed at 1141 cm^{-1}, associated with the PVA polymer, signifies the C-O stretching bond. Interestingly, 1323 cm, the expected peak, usually associated with the PAAm polymer, was absent in these spectra. Instead, several peaks were detected at 1240.67, 1240.68, 1240.61, 1240.40 and 1239.69 cm^{-1}, indicating (C-O) stretching [29, 30]. A significant change in the C -H stretch area is also clear, which represents the contribution from both PVA and PAAm polymer. The observed peaks are located at 2895.29, 2893.09, 2890.43, 2891.25, and 2891.20 cm^{-1}, rather than the typical 2940 cm^{-1} and 2931 cm^{-1} bands commonly linked to the same polymer. These peaks also correspond to (C-H) stretching vibrations. Furthermore, a distinct shift is observed in the (C=O) stretching bond, indicating the presence of the PVA polymer. This shift leads to peaks at 1732.71 and 1733.16 cm^{-1}, rather than the usual 1731 cm^{-1} bond associated to the same polymer, which is also attributed to (C=O) stretching. Additionally, there is a similar shift in the (C-C) stretching bond for the PVA polymer. The newly observed peaks appear at 1090.50, 1099.82, 1107.07, and 1101.25 cm^{-1}, rather than the standard 1087 cm^{-1} bond typically associated with (C-C) stretching as noted in these studies [30, 31]. There is a clear reduction in transmittance as the concentration of CNT increases. Higher film density leads to a greater concentration of atoms and ions along the light path. which intensifies absorbance within the UV and IR regions. This behavior is depicted in Figure 2 and the associated images (B, C, D, and E). FTIR analysis suggests that no chemical reaction occurs between the carbon nanotubes (CNT) and the polymeric blend. Instead, the interaction appears to be a result of purely physical blending. This interpretation is supported by the absence of specific bonds associated with the nanocomposite and the lack of additional peaks in the IR spectra. These conclusions are consistent with previous research findings [32].

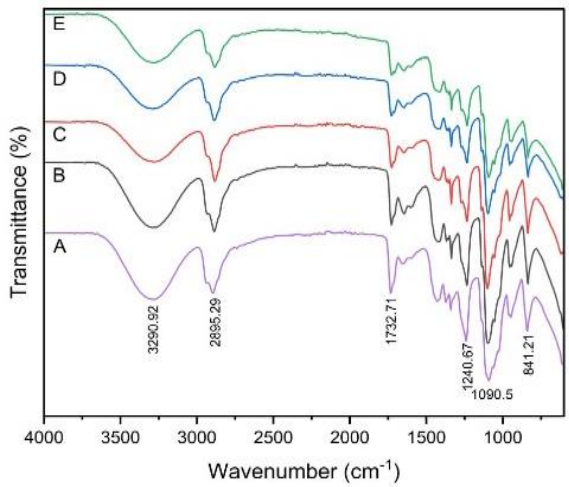

Figure 1. FTIR spectra of PVA-PAAm-PEG:CNT with various content of CNT: (A) 0 wt.% (B) 0.5 wt.% (C) 1 wt.% (D) 1.5 wt.% and (E) 2 wt.%

Figure 2 presents scanning electron microscopy (SEM) micrographs of PVA-PAAm-PEG blend films and PAAm-PVA-PEG:CNT nanocomposite films captured at a magnification of 7000x. Micrographs labeled A and B illustrate a smooth, uniformly distributed morphology characterized by a relatively soft surface texture. In contrast, the micrographs labeled C, D, and E exhibit discernible alterations in surface morphology alongside an increase in surface roughness proportional to the rising CNT content within the PAAm-PVA-PEG:CNT nanocomposite matrix. The nanocomposite films display well-dispersed CNTs without visible signs of aggregation, indicating a homogenous growth mechanism. SEM analysis further reveals that the

CNTs integrated into the nanocomposite surface possess average dimensions of approximately 339.7 nm. The findings are consistent with the optical microscopy images.

Figure 3 illustrates the ultraviolet-visible absorption spectra of PVA-PAAm-PEG:CNT nanocomposites containing varying concentrations of CNTs, documented across the wavelength spectrum of 200–800 nm at ambient temperature. The spectra unequivocally demonstrate that all samples exhibit substantial absorbance in the ultraviolet (UV) region.

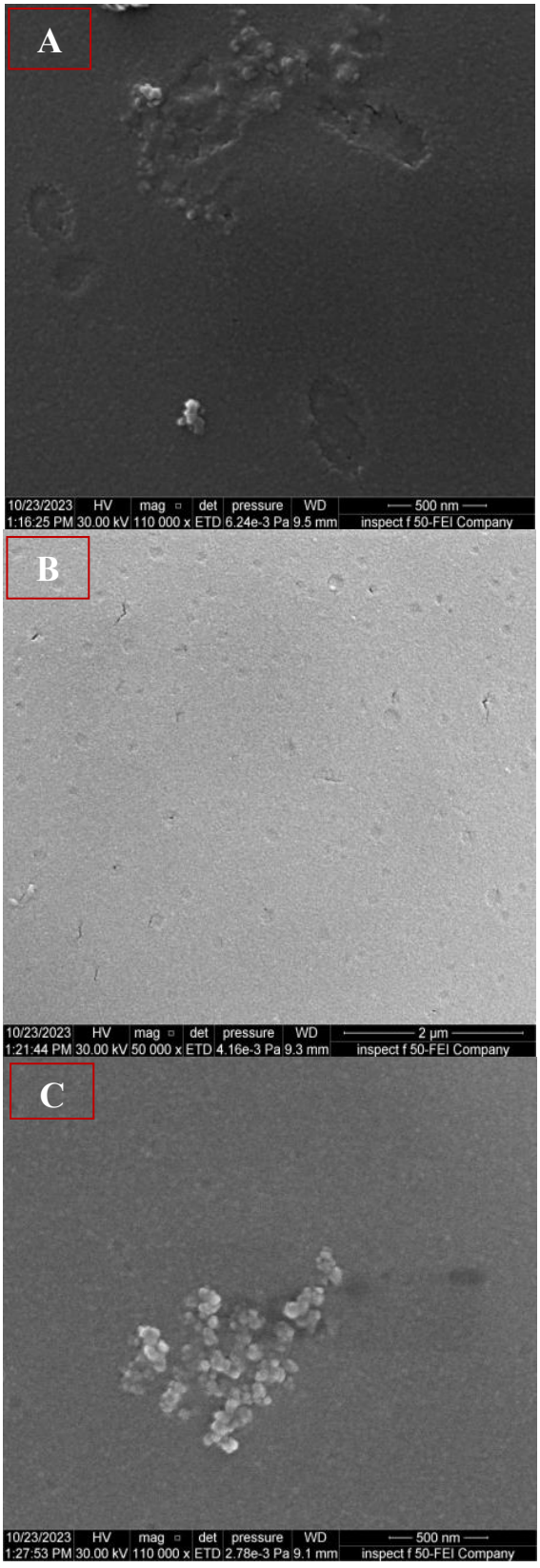

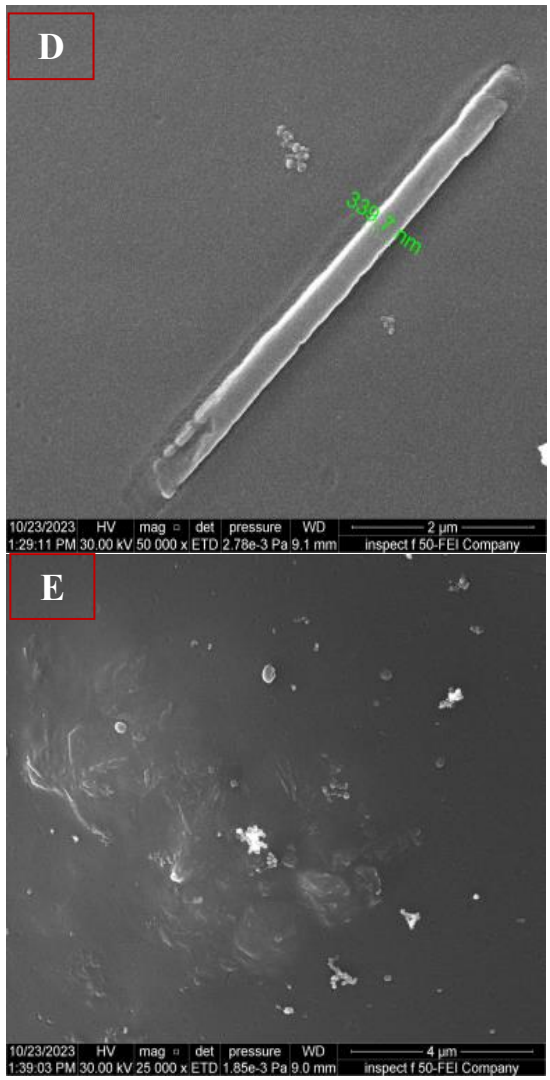

Figure 2. SEM images of PVA-PAAm-PEG:CNT with various contents of CNT and magnifications (A) 0 wt.% (B) 0.5 wt.% (C) 1 wt.% (D) 1.5 wt.% and (E) 2 wt.%

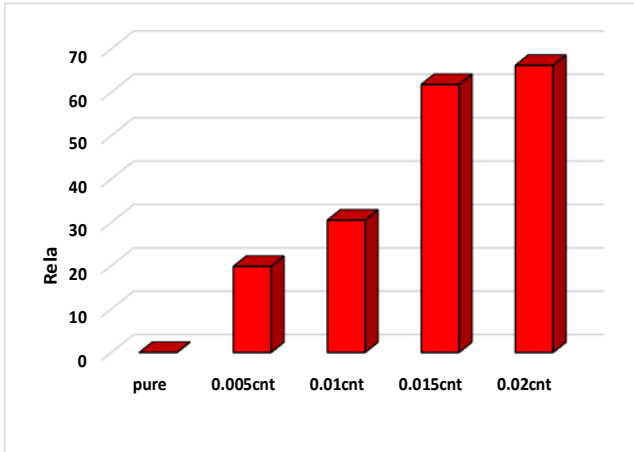

Figure 3. The absorbance spectra as a function of wavelength of PVA-PAAm-PEG blend and PVA-PAAm-PEG:CNT nanocomposites

The spectra clearly indicate that all samples exhibit significant absorption in the ultraviolet (UV) region, whereas absorbance significantly diminishes in the visible range. This optical behavior can be explained by the interaction dynamics between incident photons and the material. At longer

wavelengths in the visible spectrum, the photon energy is insufficient to engage with the material's atomic structure, thereby allowing photons to traverse the film with minimal absorption. In contrast, as the wavelength decreases and nears the material's fundamental absorption edge, photon energy becomes adequate to induce enhanced interactions with the material, resulting in a substantial increase in absorbance. Furthermore, the absorbance intensifies with the progressive increment of CNT content. This augmentation is attributed to the higher capacity of free electrons in the nanomaterials to absorb incident light more effectively. The findings align closely with previously reported results [33], reinforcing the consistency of these observations.

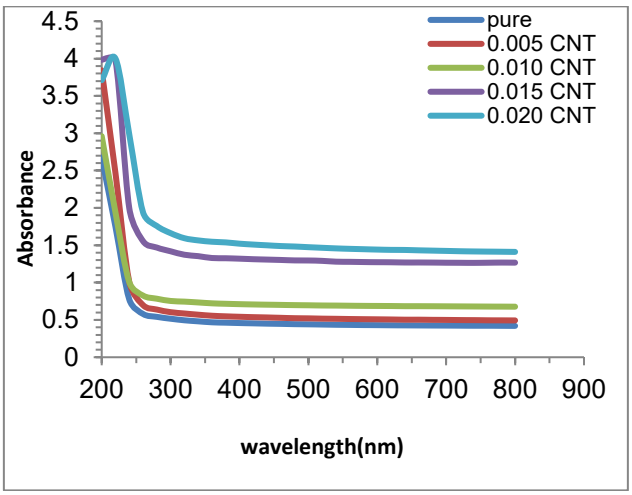

Figure 4. The relative error as a function of concentration of PVA-PAAm-PEG blend and PVA-PAAm-PEG:CNT nanocomposites

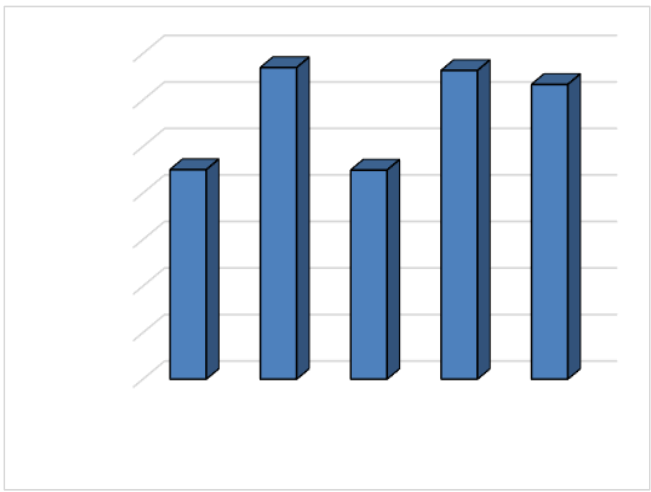

Figure 5. The standard deviation as a function of concentration of PVA-PAAm-PEG blend and PVA-PAAm-PEG:CNT nanocomposites

The statistical analysis illustrated in Figure 4 and Figure 5 highlights the absorption spectrum, revealing clear and consistent trends in absorbance, absorption coefficient, energy gap, and refractive index as the concentration of CNT increases. Notably, the data shows a rise in both standard deviation and error percentage, as shown in Table 2, emphasizing the pronounced impact of CNT on the optical properties.

Table 2. The standard deviation and relative error values in PVA-PAAm-PEG:CNT nanocomposites

Sample	%Error	StdDev
Pure	0	0.4503
0.005CNT	19.84541	0.6698
0.01CNT	30.50729	0.4495
0.015CNT	61.79583	0.6635
0.02CNT	66.20241	0.6335

The absorption coefficient of the polymer mixture and its corresponding nanocomposite films was determined in the high absorption region near the fundamental absorption edge, applying Lambert-Beer's law [34]. This relationship is given by:

$$\alpha = 2.303 \frac{A}{t} \quad (1)$$

In this formula, (A) represents the sample's absorbance, while (t) denotes its thickness. Figure 6 illustrates the relationship between the absorption coefficient (α) and photon energy for the PVA-PAAm-PEG polymer mixture, incorporating varying concentrations of carbon nanotubes (CNTs). The plot reveals that at lower photon energies, the absorption coefficient remains at minimal levels, indicating a lower probability of electron excitation. This result is primarily attributable to the inadequate photon energy required to elevate electrons from the valence band to the conduction band.

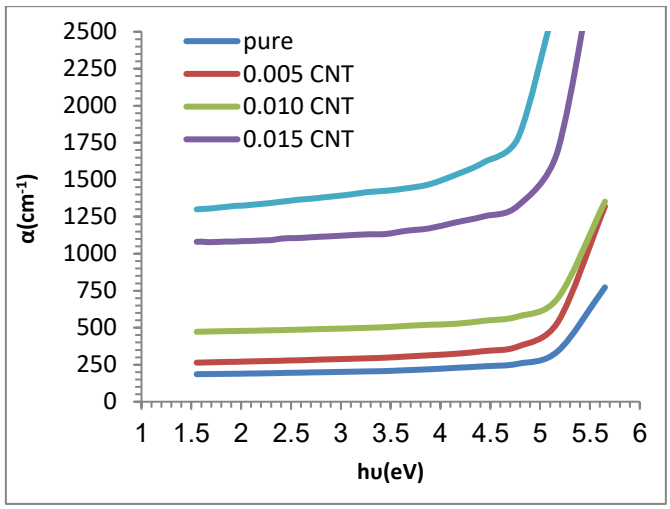

Figure 6. Relationship between the absorption coefficient and energy of PVA-PAAm-PEG blends and PVA-PAAm-PEG:CNT nanocomposites

Conversely, as photon energy increases, the absorption coefficient escalates sharply. Signifying a higher likelihood of electron excitation. Such behavior occurs when photon energies surpass the ccminant, ensuring conservation of both energy and momentum between photons and electrons. At lower absorption coefficient values ($\alpha < 10^4$ cm^{-1}) associated with reduced photon energies, indirect electronic transitions dominate. This regime relies on phonon interactions to maintain electron motion conservation, showcasing a fundamentally different excitation mechanism. These observations are consistent with earlier studies and are in agreement with established findings reported in this research [35].

The energy band gaps of the films were determined utilizing the Tauc relation, as expressed in Eq. (2) [36, 37]. This formulation incorporates the relationship:

$$\alpha h\upsilon = B(h\upsilon - Eg^{opt} \pm E_{ph})^{r} \quad (2)$$

Here, E_{ph} represents the phonon energy, with the negative sign (-) corresponding to phonon absorption and the positive sign (+) signifying phonon emission. The parameter (r), known as the exponential constant, varies based on the nature of the electronic transitions: (r = 2) is applicable to allowed indirect transitions, while (r = 3) pertains to forbidden indirect transitions. When (r = 2), the calculation yields the energy band gap for an allowed indirect transition, whereas for (r =3), it corresponds to a forbidden indirect transition [30].

Figure 7 illustrates the relationship between the square root of absorption edge, $(\alpha hv)^{1/2}$ and photon energy for PVA-PAAm-PEG:CNT nanocomposites. By extrapolating a straight line from the upper region of the curve to intersect the x-axis at $(\alpha hv)^{1/2} = 0$, the energy band gap for allowed indirect transitions was determined [38]. The resulting values are summarized in Table 3.

The research indicates that the energy band gap diminishes with an increase in the weight percentage of CNT. This decrease can be ascribed to the emergence of localized states within the forbidden energy gap. The electronic transition process transpires in two phases: electrons are elevated from the local levels of the valence band and subsequently ascend to the conduction band as the CNT content increases. This behavior underscores the heterogeneous characteristics of nanocomposites, wherein electronic conductivity is contingent upon the incorporated materials. Increased CNT concentrations establish conductive pathways within the polymer matrix, enhancing electron transfer from the valence band to the conduction band. Thus, this explains the decrease in energy band gap with the augmentation of CNT content.These results align with previous research in this study [39].

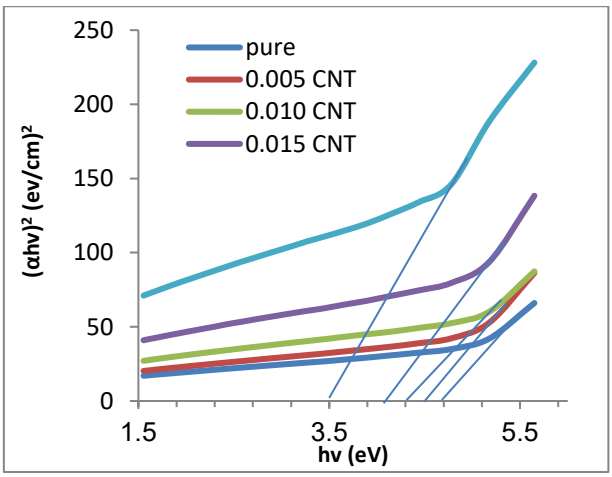

Figure 7. Optical energy gap of the allowed indirect transition with the energy of PVA-PAAm-PEG:CNT nanocomposites

The refractive index (n) is determined using Eq. (3) [40]:

$$n = \sqrt{\frac{4R - k^2}{(R-1)^2}} - \frac{R+1}{R-1} \quad (3)$$

Figure 8 shows how the refractive index varies with wavelength for the PVA-PEG: CNT nanocomposite. The findings indicate an increase in the refractive index as the weight fraction of the polymer matrix rises. This data is largely attributed to the density of nanostructures due to the addition of carbon nanotubes (CNTs). Furthermore, the optical properties of the material, particularly regarding light transmission, are significantly improved, especially in regions where the refractive index is higher within the ultraviolet (UV) spectrum. These insights are consistent with previous research findings [41].

Table 3. The energy gap values corresponding to the allowed indirect transition in PVA-PAAm-PEG:CNT nanocomposites

Samples	Allowed Indirect Transition (eV)
PVA-PAAm-PEG	4.7
PVA-PAAm-PEG 0.5% CNT	4.5
PVA-PAAm-PEG 1% CNT	4.3
PVA-PAAm-PEG 1.5% CNT	4.1
PVA-PAAm-PEG 2% CNT	3.5

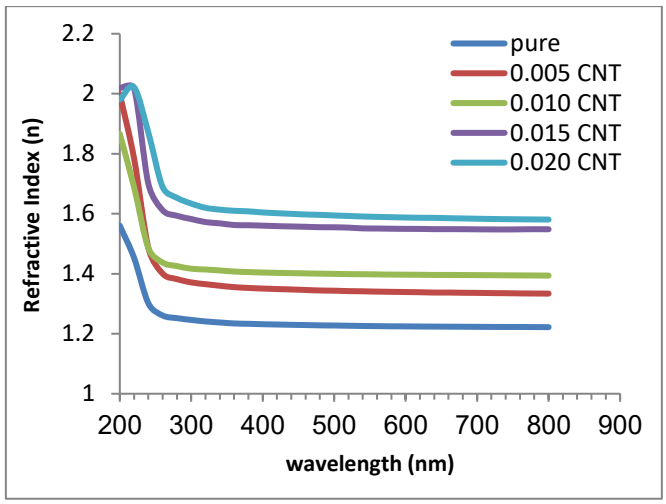

Figure 8. The refractive index (n) as a function of wavelength of PVA-PAAm-PEG blend and PVA-PAAm-PEG:CNT nanocomposites

The dielectric constant is calculated using the following Eq. (4) [42]:

$$\acute{\varepsilon} = Cp\ d/\ \varepsilon_o\ A \quad (4)$$

Here, Cp represents the capacitance of the material, d refers to the thickness (120 µm), and A refers to the area (1 cm²).

Figure 9 showcases the dominant dielectric constant values for PVA-PAAm-PEG and its nanocomposite films containing varying concentrations of carbon nanotubes (CNTs) at 0.5%, 1.0%, 1.5%, and 2.0% wt.%. The measurements were performed as a function of applied electrical field frequency. The data indicate that, across all samples, the dielectric constant decreases with increasing frequency.

The data reveal a consistent trend across all samples: the dielectric constant diminishes as frequency increases. This phenomenon occurs because vacuum charges fail to adapt swiftly to fluctuations in the electric field, resulting in reduced

dielectric constant values and diminished vacuum charge polarization. Additionally, at elevated frequencies, ions are unable to respond promptly to changes in the electric field, thereby lowering their influence on the dielectric constant. In such conditions, electron polarization emerges as the dominant factor driving the dielectric response, further contributing to the observed decrease in the dielectric constant. Conversely, at lower frequencies, space charge polarization plays a more significant role in the overall dielectric response.

The highest dielectric constant values recorded at 100 Hz are as follows: 0.40 for 0.5 wt% CNT, 0.46 for 1.0 wt% CNT, 0.53 for 1.5 wt% CNT, and further increments up to 0.70 for 2.0 wt% CNT. These findings underscore the enhanced energy storage capability of the material, as evidenced by the increasing dielectric constant with higher CNT concentrations under external electric fields.

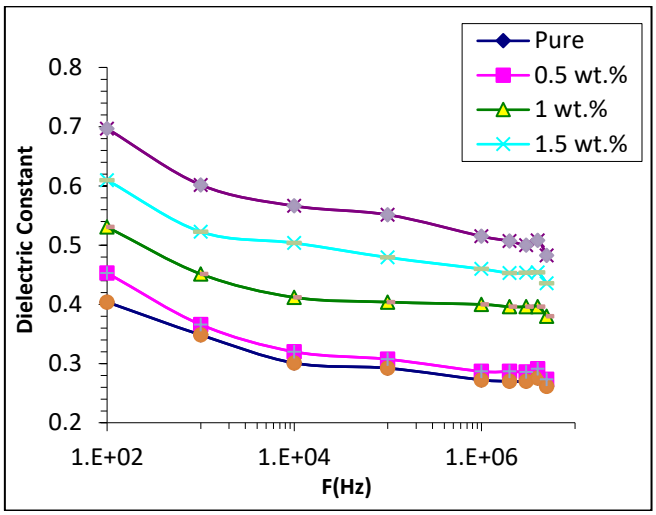

Figure 9. Variation of dielectric constant Wavelength of PVA-PAAm-PEG Blend and PVA-PAAm-PEG:CNT nanocomposite with frequency at RT

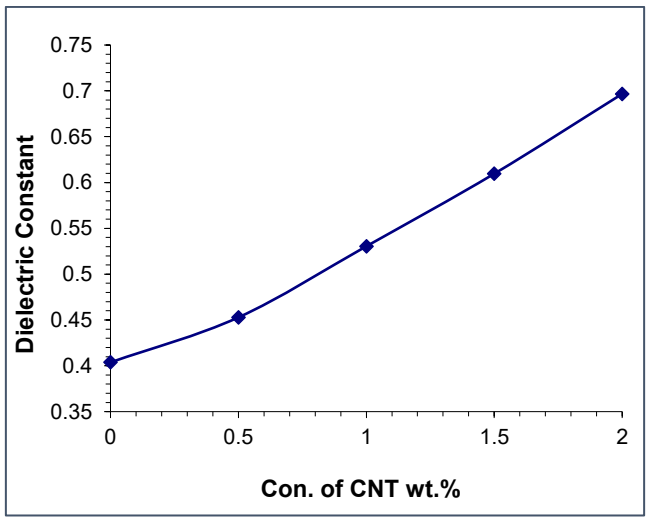

Figure 10. Effect of CNT concentrations on dielectric constant of PVA-PAAm-PEG Blends at 100Hz

Figure 10 illustrates the variation in the dielectric constant as a function of CNT concentration at a frequency of 100 Hz. The results demonstrate a upward trend in dielectric behavior with increased CNT content in the nanocomposite films. This enhancement is primarily attributed to the interfacial polarization effects occurring within the nanocomposites under an alternating electric field. Additionally, the greater availability of charges introduced by the presence of CNTs contributes significantly to the rise in dielectric constant values, thereby improving the material's electrical performance and energy storage capabilities [43].

Dielectric loss represents the electrical energy dissipated within a material due to an applied electric field, which is converted into thermal energy. The dielectric loss for nanocomposites is calculated using the following Eq. (5) [44]:

$$\varepsilon'' = \acute{\varepsilon}\, D \tag{5}$$

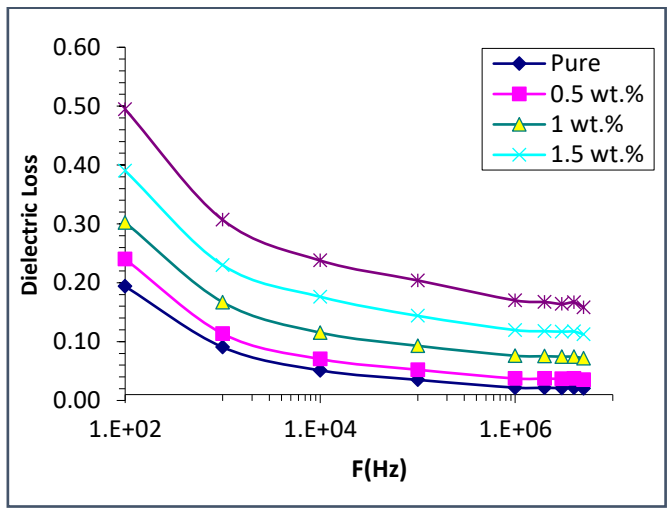

Figure 11. Variation of dielectric loss of PVA-PAAm-PEG Blend and PVA-PAAm-PEG:CNT nanocomposite with frequency at RT

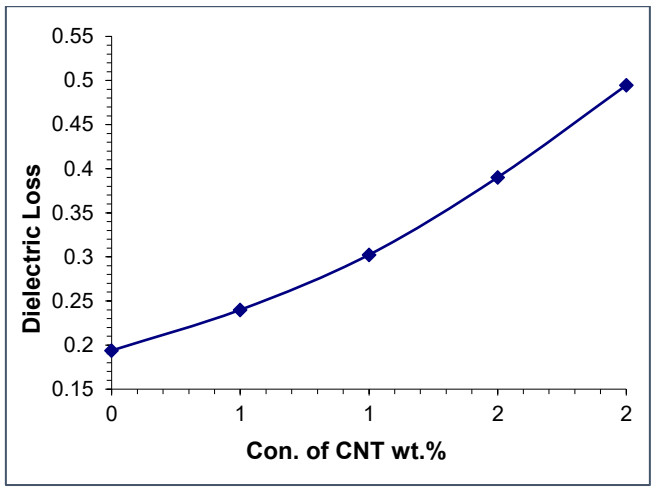

Figure 12. Effect of CNT concentrations on dielectric loss of (PVA-PAAm-PEG) blends at 100Hz

The dependence of dielectric loss on the electric field frequency for carbon nanotubes (CNTs) embedded in (PVA-PAAm-PEG) blends at room temperature (RT) is depicted in Figure 11. The results indicate that the dielectric loss of the nanocomposites decreases as the frequency of the applied electric field increases for all samples. This trend is attributed to the reduced contribution of space charge polarization at higher frequencies. Among the samples, nanocomposite films containing 2 wt.% CNTs exhibit the highest dielectric loss, recorded at 0.49, at a low frequency of 102 Hz.

Similarly, Figure 12 highlights a correlation between the dielectric loss of CNT-based nanocomposites and nanoparticle concentration, showing an increase in dielectric loss with rising nanoparticle content. This phenomenon is ascribed to the enhanced availability of charge carriers within the material. Comparable behavior has been documented in the study [45].

The A.C. electrical conductivity (σA.C) of nanocomposites is determined using the Eq. (6) [46]:

$$\sigma_{A.C} = 2\pi f \acute{\varepsilon} D \varepsilon_o \quad (6)$$

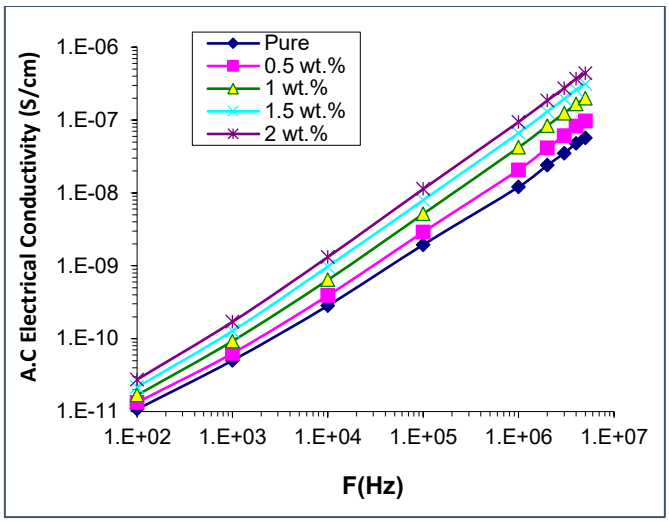

Figure 13. Variation of A.C. electrical conductivity of PVA-PAAm-PEG Blend and PVA-PAAm-PEG:CNT nanocomposite with frequency at RT

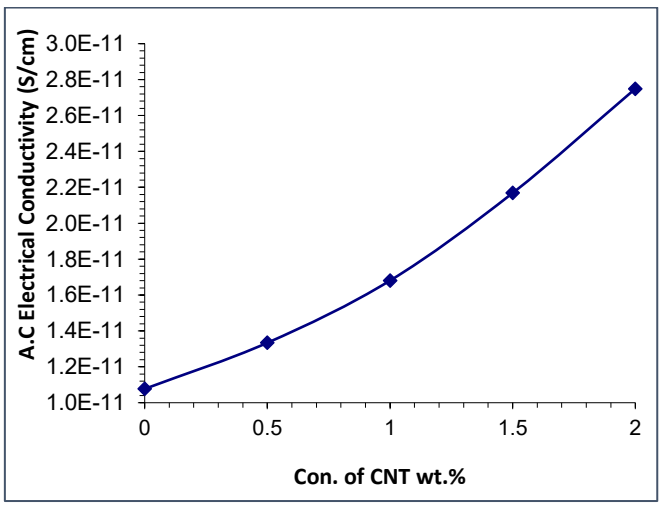

Figure 14. Effect of CNT nanoparticles concentrations on A.C. electrical conductivity of (PVA-PAAm-PEG) blend at 100Hz

The variation of A.C. electrical conductivity with the frequency of the electric field is illustrated in Figure 13 for carbon nanotubes (CNT) embedded within PVA-PAAm-PEG blends at room temperature (RT). The results indicate a substantial increase in A.C. conductivity as the frequency of the applied electric field rises for all samples. This behavior can be attributed to the polarization of space charges at lower frequencies and the hopping mechanism of charge carriers [47].

Additionally, Figure 14 highlights the conductivity of the PVA-PAAm-PEG blends at a frequency of 102 Hz, which shows a proportional increase with the rising weight percentage of CNT. Incorporating nanoparticles into the nanocomposite composition enhances conductivity by boosting the number of charge carriers. This effectively reduces the material's resistance, consequently increasing its A.C. electrical conductivity. Similar findings have been reported in the study [48].

5. ANTI-BACTERIAL ACTIVITY APPLICATION

Nanoparticles are emerging as a promising alternative to conventional antibiotics due to their ability to deliver broad-spectrum antibacterial effects even at low concentrations. This study investigates the antibacterial efficacy of nanocomposites incorporating PVA-PAAm-PEG blended with varying amounts of carbon nanotubes (CNTs) at concentrations of 0, 0.5, 1.5, and 2 wt.%. The experiments were conducted using *Escherichia coli* strain ATCC 25922, a prominent standard strain for evaluating antibacterial activity. Bacterial samples were grown on LB agar plates and incubated at 37°C for 24 hours under strictly controlled conditions using a temperature regulator. To prepare the bacterial suspension, sterile saline was utilized to achieve a uniform concentration equivalent to the 0.5 McFarland standard. Antibacterial activity was determined through the disk diffusion method, where disks impregnated with the antibacterial agent were placed on the agar medium. After a 24-hour incubation period, the inhibition zones were measured to assess effectiveness. Observations revealed substantial variations in inhibition zone sizes between bacteria exposed solely to the polymer blend and those treated with its nanocomposite formulations, as illustrated in Figure 15. These findings strongly highlight the enhanced antibacterial potential of nanocomposites over their pure polymer counterparts.

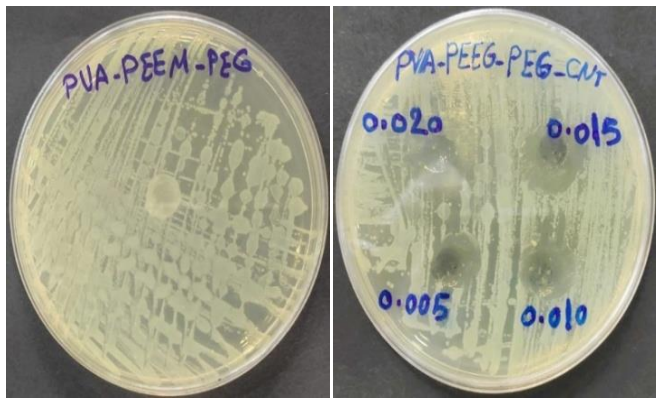

Figure 15. Images for inhibition zones of PVA-PAAm-PEG blend and PVA-PAAm-PEG:CNT nanocomposites on *E. coli*

While the pure polymer blend exhibited no antibacterial activity, the incorporation of nanoparticles into the polymer matrix markedly improved bacterial resistance inhibition. The findings highlight that nanocomposite films demonstrate substantial efficacy in inhibiting **E. coli** growth. This enhanced antibacterial activity is primarily attributed to the generation of reactive oxygen species (ROS), which induce oxidative stress through reactive oxygen radicals. ROS, such as hydroxyl radicals (-OH) and superoxide radicals (O^{2-}),

inflict damage on bacterial DNA and proteins, thereby compromising bacterial viability [49, 50]. Furthermore, the interaction between nanoparticles within the nanocomposites and bacterial cells initiates electromagnetic processes that facilitate oxidation, leading to rapid bacterial extermination. This effect is a result of the positively charged nanocomposites interacting with the negatively charged bacterial membranes [51, 52]. Such findings underscore the significant potential of these materials for advancing biosensor technologies and developing highly effective antibacterial disinfectants, offering promising avenues for future research and practical applications.

6. CONCLUSIONS

The PVA-PAAm-PEG:CNT blend was successfully synthesized through the casting method. Optical microscopy demonstrated a uniform and highly integrated dispersion of nanomaterials across the films, ensuring structural consistency. FTIR analysis revealed notable shifts in specific bands and changes in intensity compared to the PVA-PAAm blend film, signaling strong molecular interactions. Scanning electron microscopy (SEM) provided intricate details about the compatibility between polymer components and nanomaterials, while also offering a closer examination of the surface morphology of the PVA-PAAm-PEG:CNT nanocomposite films. Notably, an increase in CNT content was associated with reduced permeability levels. The optical properties, including absorbance, absorption coefficient, and refractive index, exhibited a rise with higher CNT concentrations. Simultaneously, the optical energy gap decreased progressively from 4.7 eV to 3.5 eV as the CNT content increased. Regarding electrical characteristics, the dielectric constant and dielectric loss of the nanocomposites showed consistent growth with increasing CNT levels but displayed a decline at higher applied electric field frequencies. Conversely, A.C. conductivity exhibited a significant boost with elevated electric field frequencies across all samples. This improvement in conductivity was particularly prominent at 102 Hz when using higher CNT weight proportions, attributed to an increased number of charge carriers. In addition, the rise in nanoparticle content within the PVA-PAAm-PEG:CNT films contributed to an expanded inhibition zone diameter against *Escherichia coli*, indicating heightened antibacterial effectiveness and broadening its potential for antimicrobial applications. These properties make PVA-PAAm-PEG:CNT blends versatile, with applications spanning a wide range of industries, including automotive, aerospace, electronics, and medical devices.

7. SUGGESTION FOR FUTURE WORK

- Study the effect of PVA-PAAm-PEG:CNT blends on living cells to determine their safety and effectiveness.
- Improve the properties of PVA-PAAm-PEG:CNT blends by modifying their composition or adding other materials.
- Expand the application of PVA-PAAm-PEG:CNT blends to other fields, such as the electronics industry and renewable energy.

ACKNOWLEDGMENT

The authors extend their heartfelt appreciation to the College of Education for Pure Sciences at the University of Babylon, Iraq, for providing essential resources and support.

REFERENCES

[1] Kadim, A.M., Abdulkareem, A.D., Alrubaie, A.J.K., Abass, K.H. (2023). Formation of PVA-PMMA-PAAm blend with various content of dextrin for drug delivery application. Materials Today: Proceedings, 80(3): 2474-2479. https://doi.org/10.1016/j.matpr.2021.06.391

[2] Molaei, P., Kazeminezhad, I. (2019). One-step in situ synthesis of antimony sulfide/reduced graphene oxide composite as an absorber layer with enhanced photocurrent performances for solar cells. Journal of Nanoparticle Research, 21(2): 54. https://doi.org/10.1007/s11051-019-4490-9

[3] Firdaus, R.M., Rosli, N.I.M., Ghanbaja, J., Vigolo, B., Mohamed, A.R. (2019). Enhanced adsorption of methylene blue on chemically modified graphene nanoplatelets thanks to favorable interactions. Journal of Nanoparticle Research, 21(4): 257. https://doi.org/10.1007/s11051-019-4701-4

[4] Debelak, B., Lafdi, K. (2007). Use of exfoliated graphite filler to enhance polymer physical properties. Carbon, 45(9): 1727-1734. https://doi.org/10.1016/j.carbon.2007.05.010

[5] Khammassi, S., Tarfaoui, M. (2020). Influence of exfoliated graphite filler size on the electrical, thermal, and mechanical polymer properties. Journal of Composite Materials, 54(25): 3731-3741. https://doi.org/10.1177/0021998320918639

[6] Mark, J.E. (2001). Polymer Data Handbook. 2nd ed. New York, USA: Oxford University Press, Inc.

[7] Razzak, M.T., Darwis, D., Zainuddin, Sukirno. (2021). Irradiation of polyvinyl alcohol and polyvinyl pyrrolidone blended hydrogel for wound dressing. Radiation Physics and Chemistry, 62(1): 107-113. https://doi.org/10.1016/S0969-806X(01)00427-3

[8] Dash, M., Chiellini, F., Ottenbrite, R.M., Chiellini, E. (2011). Chitosan-A versatile semi-synthetic polymer in biomedical applications. Progress in Polymer Science, 36(8): 981-1014. https://doi.org/10.1016/j.progpolymsci.2011.02.001

[9] Zbala, A.A.K., Al-Ogaili, A.O.M., Abass, K.H. (2022). Effect of adding silver nanoparticles on structural and microscopic properties of PAAm-PEG polymer blend. Journal of Nanostructures, 12(4): 892-897. https://doi.org/10.22052/JNS.2022.04.011

[10] Rajendran, S., Sivakumar, M., Subadevi, R. (2004). Investigations on the effect of various plasticizers in PVA–PMMA solid polymer blend electrolytes. Materials Letters, 58(5): 641-649. https://doi.org/10.1016/S0167-577X(03)00585-8

[11] Lee, J.H., Lee, H.B., Andrade, J.D. (1995) Blood compatibility of polyethylene oxide surfaces. Progress in Polymer Science, 20(6): 1043-1079. https://doi.org/10.1016/0079-6700(95)00011-4

[12] Kadim, A.M., Abass, K.H., Abdali, K., Musa, S.J. (2024). Effect of loading corn starch nanoparticles on the morphological, optical, and dielectric behaviors of

PVA/PMMA/PAAm polymer blend for optoelectronic and antibacterial applications. Nano Biomedicine and Engineering, 16(1): 119-127. https://doi.org/10.26599/NBE.2024.9290049
[13] Buchholz, F.L. (2015). Polyacrylamides and poly(acrylic acids). Ullmann's Encyclopedia of Industrial Chemistry. https://doi.org/10.1002/14356007.a21_143
[14] Zbala, A.A.K., Al-Ogaili, A.O.M., Abass, K.H. (2022). Optical properties and dispersion parameters of PAAm-PEG polymer blend doped with antimony (III) oxide nanoparticles. NeuroQuantology, 20(2): 62-68. https://doi.org/10.14704/nq.2022.20.2.NQ22026
[15] Chieng, B.W., Ibrahim, N.A., Yunus, W.M.Z.W., Hussein, M.Z. (2014). Poly(lactic acid)/Poly(ethylene glycol) polymer nanocomposites: Effects of graphene nanoplatelets. Polymers, 6(1): 93-104. https://doi.org/10.3390/polym6010093
[16] Nadarajah, K. (2005). Development and characterization of antimicrobial edible films from crawfish chitosan. PhD Dissertation. Louisiana State University and Agricultural & Mechanical College.
[17] Abass, K.H., Kadim, A.M., Mohammed, S.K., Agam, M.A. (2021). Drug delivery systems based on polymeric blend: A review. Nano Biomedicine and Engineering, 13(4): 414-424. https://doi.org/10.5101/nbe.v13i4.p414-424
[18] Klein, R. (2012). Laser Welding of Plastics. John Wiley and Sons.
[19] Amin, S., Amin, M. (2011). Thermoplastic elastomeric (Tpe) materials and their use in outdoor electrical insulation. Reviews on Advanced Materials Science, 29(3): 15-30. https://www.ipme.ru/e-journals/RAMS/no_12911/02_amin.pdf.
[20] Cowie, J.M.G., Arrighi, V. (1991). Polymers: Chemistry and Physics of Modern Materials. Glasgow. CRC Press. https://doi.org/10.1201/9781420009873
[21] Scobbo, J.J., Goettler, L.A. (2003). Applications of Polymer Alloys and Blends. In: Utracki, L.A. (eds) Polymer Blends Handbook. https://doi.org/10.1007/0-306-48244-4_13
[22] Lakouraj, M.M., Norouzian, R., Tavakoli, M. (2023). Synthesis, characterization, and properties of sulfonated CNT-doped poly(aniline-*co*-carbazole)-PVA conductive films. Macromolecular Materials and Engineering, 308(77): 2200696. https://doi.org/10.1002/mame.202200696
[23] Mi, D., Zhao, Z., Bai, H. (2023). Effects of orientation and dispersion on electrical conductivity and mechanical properties of carbon nanotube/polypropylene composite. Polymers, 15(10): 2370. https://doi.org/10.3390/polym15102370
[24] Nasar, G., Khalil, U., Khan, M.S., Nadeem, Q. (2022). Synthesis and characterization of CNT/PVA nanocomposites for electrical, thermal and morphological properties. Journal of Materials and Physical Sciences, 3(1): 14-21. https://doi.org/10.52131/jmps.2022.0301.0022
[25] Yue, Y., Xu, K., Liu, X., Chen, Q., Sheng, X., Wang, P. (2008). Preparation and characterization of interpenetration polymer network films based on poly(vinyl alcohol) and poly(acrylic acid) for drug delivery. Journal of Applied Polymer Science, 108(6): 3836-3842. https://doi.org/10.1002/app.28023
[26] Manjunath, A., Deepa, T., Supreetha, N.K., Irfan, M. (2015). Studies on AC electrical conductivity and dielectric properties of PVA/NH_4NO_3 solid polymer electrolyte films. Advances in Materials Physics and Chemistry, 5(2): 295-301. https://doi.org/10.4236/ampc.2015.58029
[27] Rasheed, M.H., Hashim, F.S., Abass, K.H. (2023). Impact of Ag nanoparticles on the spectral and optical properties of electrospun nanofibrous poly(vinyl alcohol)-poly(acrylamide). International Journal of Nanoscience, 22(3): 2350025. https://doi.org/10.1142/S0219581X23500254
[28] Deshmukh, K., Ahmad, J., Hägg, M.B. (2014). Fabrication and characterization of polymer blends consisting of cationic polyallylamine and anionic polyvinyl alcohol. Ionics, 20(7): 957-967. https://doi.org/10.1007/s11581-013-1062-3
[29] Dweik, H., Sultan, W., Sowwan, M., Makharza, S. (2008). Analysis characterization and some properties of polyacrylamide copper complexes. International Journal of Polymeric Materials, 57(3): 228-244. https://doi.org/10.1080/00914030701413280
[30] Yu, J.C., Zhao, F.G., Shao, W., Ge, C.W., Li, W.S. (2015). Shape-controllable and versatile synthesis of copper nanocrystals with amino acids as capping agents. Nanoscale, 7(19): 8811-8818. https://doi.org/10.1039/c5nr00146c
[31] Mansur, H.S., Sadahira, C.M., Souza, A.N., Mansur, A.A.P. (2008). FTIR spectroscopy characterization of poly(vinyl alcohol) hydrogel with different hydrolysis degree and chemically crosslinked with glutaraldehyde. Materials Science and Engineering, 28(4): 539-548. https://doi.org/10.1016/j.msec.2007.10.088
[32] Luo, Y.L., Chen, L.L., Xu, F., Feng, Q.S. (2012). Fabrication and characterization of copper nanoparticles in PVA/PAAm IPNs and swelling of the resulting nanocomposites. Metals and Materials International, 18(5): 899-908. https://doi.org/10.1007/s12540-012-5024-5
[33] Chiad, S.S., Alkelaby, A.S., Sharba, K.S. (2020). Optical conduct of nanostructure Co_3O_4 rich highly doping Co_3O_4: Zn alloys. Journal of Global Pharma Technology, 11(7): 662-665.
[34] Alkelaby, A.S., Abass, K.H., Mubarak, T.H., Habubi, N.F., Chiad, S.S., Al-Baidhany, I. (2019). Effect of MnCl2 additive on optical and dispersion parameters of poly methyl methacrylate films. Journal of Global Pharma Technology 11(4): 347-352. https://www.researchgate.net/publication/334645612
[35] Alrowaili, Z.A., Echeweozo, E.O., Kırkbınar, M., Çalışkan, F., Alzahrani, J.S., Al-Buriahi, M.S. (2024). Effect of bismuth oxide on radiation shielding and interaction characteristics of polyvinyl alcohol-based polymer: Potential use in medical apron design. Journal of Radiation Research and Applied Sciences, 17(4): 101162. https://doi.org/10.1016/j.jrras.2024.101162
[36] Hao, Y., Shih, H., Munoz, Z., Kemp, A., Lin, C.C. (2014). Visible light cured thiol-vinyl hydrogels with tunable degradation for 3D cell culture. Acta Biomaterialia, 10(2): 104-114. https://doi.org/10.1016/j.actbio.2013.08.044
[37] Al-Jamal, A.N., Karar Abdali, O., Abbass, K.H., Rabee, B.H., Al-Bermany, E. (2023). Silver NPs reinforced the structural and mechanical properties of PVA-PAAm-PEG nanocomposites. AIP Conference Proceedings,

2414: 030005. https://doi.org/10.1063/5.0114621
[38] Al-Jamal, A.N., Hadi, Q.M., Hamood, F.J., Abass, K.H. (2019). Particle size effect of Sn on structure and optical properties of PVA-PEG blend. In Proceedings - International Conference on Developments in eSystems Engineering (DeSE), Kazan, Russia, pp. 736-740. https://doi.org/10.1109/DeSE.2019.00137
[39] Asadi, S.M.A., Hamood, F.J., Abass, K.H., Mohammed, S.K., Hassan, I.M., Latif, D. (2019). The effect of MgO nanoparticles on structure and optical properties of PVA-PAAm blend. Research Journal of Pharmacy and Technology, 12(6): 2768-2771. https://doi.org/10.5958/0974-360X.2019.00464.5
[40] Abass, K.H., Obaid, N.H. (2019). 0.006wt.%Ag-doped Sb2O3 nanofilms with various thickness: Morphological and optical properties. Journal of Physics: Conference Series, 1294(2): 022005. https://doi.org/10.1088/1742-6596/1294/2/022005
[41] Sharba, K.S., Alkelaby, A.S., Sakhil, M.D., Abass, K.H., Habubi, N.F., Chiad, S.S. (2020). Enhancement of urbach energy and dispersion parameters of polyvinyl alcohol with Kaolin additive. NeuroQuantology, 18(3): 66-73. https://doi.org/10.14704/nq.2020.18.3.NQ20152
[42] Abass, K.H., Hamed, H.A. (2020). Reduction of energy gap in ZrO_2 nanoparticles on structural and optical properties of casted PVA–PAAm blend. Journal of Green Engineering, 10(7): 4166-4176. https://doi.org/10.15407/nnn.22.02.379
[43] Sakhil, M.D., Shaban, Z.M., Sharba, K.S., Habub, N.F., Abass, K.H., Chiad, S.S., Alkelaby, A.S. (2020). Influence mgo dopant on structural and optical properties of nanostructured cuo thin films. NeuroQuantology, 18(5): 56-61. https://doi.org/10.14704/nq.2020.18.5.NQ20168
[44] Jumaah, S.H., Hussein, M.R., Habubi, N.F., Chiad, S.S., Abass, K.H. (2022). Improving the antibacterial properties of SnO_2/Mn_3O_4 hybrid thin film synthesized by spray pyrolysis method. Nano Biomedicine and Engineering, 14(3): 280-288. https://doi.org/10.5101/nbe.v14i3.p280-288
[45] Hamood, F.J., Mohmed, B.Y., Kadim, A.M., Abass, K.H., Agarwal, M.K., Mohammed, K.A. (2023). Effect of CdS nanoparticles on structural, optical and dielectric properties for gamma-ray shielding and antibacterial efficiency of PVA/PAAm polymers blend. International Journal of Nanoscience, 22(5): 2350043. https://doi.org/10.1142/S0219581X23500436
[46] Ali, R.S., Sharba, K.S., Jabbar, A.M., Chiad, S.S., Abass, K.H., Habubi, N.F. (2020). Characterization of ZnO thin film/p-Si fabricated by vacuum evaporation method for solar cell applications. NeuroQuantology, 18(1): 26-31. https://doi.org/10.14704/nq.2020.18.1.NQ20103
[47] Anju, R., Ramesan, M.T. (2024). Enhanced mechanical, electrical, thermal, and optical properties of poly(methyl methacrylate)/copper oxide nanocomposites for flexible optoelectronic devices via in-situ polymerization technique. Polymer Composites, 45(6): 5360-5371 https://doi.org/10.1002/pc.28132
[48] Shivashankar, H., Mathias, K.A., Sondar, P.R., Shrishail, M.H., Kulkarni, S.M. (2021) Study on low-frequency dielectric behavior of the carbon black/polymer nanocomposite. Journal of Materials Science: Materials in Electronics, 2(1): 28674-28686. https://doi.org/10.1007/s10854-021-07242-1
[49] Mohammed, M.K., Khudhair, T.N., Sharba, K.S., Hashim, A., Hadi, Q.M., Meteab, M.H. (2024). Tuning the morphological and optical characteristics of SnO_2/ZrO_2 nanomaterials doped PEO for promising optoelectronics applications. Revue des Composites et des Matériaux Avancés-Journal of Composite and Advanced Materials, 34(4): 495-503. https://doi.org/10.18280/rcma.340411
[50] Sharba, K.S., Alkelab, A.S., Abass, K.H. (2025). Copper oxide nanoparticles impact antibacterial activity based on electrospun PVA PEG fibers. Plasmonics. https://doi.org/10.1007/s11468-025-03062-9
[51] Yadav, L.S.R., Archana, B., Lingaraju, K., Kavitha, C., Suresh, D., Nagabhushana, H., Nagaraju, G. (2016). Electrochemical sensing, photocatalytic and biological activities of ZnO nanoparticles: Synthesis via green chemistry route. International Journal of Nanoscience, 15(4): 1650013. https://doi.org/10.1142/S0219581X16500137
[52] Alkelaby, A.S., Ahmadi, M.T., Esmaeili, A., Sedghi, H., Abass, K.H. (2024). Fabricate of one dimensional structure poly(vinyl alcohol)-polyethylene glycol: calcium fluoride nanocomposites via electrospinning technique: Characterization and antibacterial application. Polymer Bulletin, 81: 17377-17391. https://doi.org/10.1007/s00289-024-05503-7